Fission fragment mass distribution in the $^{32}S + ^{144}Sm$ reaction

T. N. Nag,[1,3] R. Tripathi,[1,3,*] S. Patra,[1] A. Mhatre,[1,3] S. Santra,[2,3] P. C. Rout,[2,3] A. Kundu,[2,3] D. Chattopadhyay,[2,3] A. Pal,[2] and P. K. Pujari[1,3]

[1]*Radiochemistry Division, Bhabha Atomic Research Centre, Mumbai 400085, India*
[2]*Nuclear Physics Division, Bhabha Atomic Research Centre, Mumbai 400085, India*
[3]*Homi Bhabha National Institute, Anushaktinagar, Mumbai 400094, India*

(Received 7 August 2020; revised 6 December 2020; accepted 15 February 2021; published 16 March 2021)

Background: An asymmetric fission was reported by Andreyev *et al.* in β-delayed fission of ^{180}Tl [Phys. Rev. Lett. **105**, 252502 (2010)]. Subsequent theoretical calculations suggested that the asymmetric nature of the mass distribution is not restricted to the ^{180}Hg only but is also expected for many other nuclei in the mass region $A \approx 180$. Thus, it is important to investigate fission fragment mass distribution for different fissioning systems over a wide range of excitation energy in the mass region $A \approx 180$.

Purpose: Present measurements have been carried out to study the nature of the fission fragment mass distribution in the $^{32}S + ^{144}Sm \rightarrow ^{176}Pt$ reaction in the compound nucleus excitation energy range of 38.7–47.5 MeV and investigate the role of multimodal fission.

Method: Mass distributions have been determined from the time of flight (TOF) of the fission fragments, which was measured with respect to the beam pulse. Two multiwire proportional counters were placed at the folding angle to detect the fission fragments. Measured TOF of the fission fragments was used to obtain their velocities, which were further used to obtain the fission fragment mass distribution.

Results: The fission fragment mass distributions at all three beam energies were observed to have flattop natures, which could not be fitted well by a one-Gaussian function. A fit using a two-Gaussian function significantly improved the χ^2 values. The ratio of the most probable heavy to light fragment mass (A_H/A_L) was observed as $\approx 99.4/76.6$. A systematic study of the centroid values of asymmetric peaks in the mass distribution for different fissioning systems around mass region $A \approx 180$ showed that heavier mass peak is centered around $A_H \approx 100$. Further analysis of A_H and A_L to obtain the corresponding neutron and proton numbers gave heavy fragment neutron number (N_H) around ≈ 56 and light fragment proton number (Z_L) in the range of ≈ 34–36.

Conclusions: Observation of the flattop nature indicated the contributions from multimodal fission having both symmetric and asymmetric fission components, similar to those reported earlier in the mass region $A \approx 180$, although it did not show a clear dip in symmetry as observed in some of the studies. The observed values of the neutron number in the heavy fragment (N_H) and proton number in the light fragment (Z_L) are consistent with the values recently proposed in Phys. Rev. C **100**, 041602(R) (2019) and arXiv:2007.16184] for fissioning systems in the similar mass range. Comparison of the data on the width of the mass distribution from the present paper with those from similar fissioning systems with different $Z_P Z_T$ values suggested that the observed width of the mass distribution has a dependence on the neutron-proton configuration along with the entrance channel dynamics.

DOI: 10.1103/PhysRevC.103.034612

I. INTRODUCTION

Fission fragment mass distribution is an important observable to understand the fusion-fission mechanisms involved in heavy-ion induced nuclear reactions along with the role of the potential-energy landscape [1–6]. In the compound nucleus (CN) fission, the nature of the mass distribution is mainly governed by the evolution of the fissioning system in a multidimensional potential-energy surface [7]. The experimental observation of asymmetric mass distributions in the low-energy fission of actinides was explained on the basis of shell and pairing corrections [8] to the potential energy calculated using the liquid drop model [9]. Gustafsson *et al.* proposed that the asymmetric mass distribution in the actinide region can be attributed to the asymmetric saddle at the outer barrier which becomes more favored compared to the symmetric saddle due to the coupling of $[40\Lambda\Omega]$ and $[51\Lambda\Omega]$ levels in the fissioning nucleus [10,11]. In the lighter fissioning systems, such as ^{210}Po, the mass distribution was predicted to be symmetric [12,13]. However, Itkis *et al.*, reported asymmetric mass distribution at an excitation energy of 30 MeV in the mass region $A \approx 200$ [14,15]. Asymmetric fission was also predicted in rare-earth fissioning systems due to the coupling of $[30\Lambda\Omega]$ and $[41\Lambda\Omega]$ levels in the fissioning nucleus making

*Corresponding author: rahult@barc.gov.in

asymmetric splitting more favorable as in the case of actinides [10,11].

The observation of asymmetric fission in β^+/EC delayed fission (βDF) of ^{180}Tl by Andreyev *et al.* [16] and Elseviers *et al.* [17] was referred to as a "new type of asymmetric fission in proton-rich nuclei" as the most probable split did not yield ^{90}Zr with $N = 50$ neutrons corresponding to spherical shell closure. Recently, Ichikawa and Moller [11] showed in their calculations that asymmetric mass distribution for ^{180}Hg can be explained in a similar way as explained for rare-earth nuclei in Ref. [10] based on the coupling of $[30\Lambda\Omega]$ and $[41\Lambda\Omega]$ levels in the fissioning nucleus. Based on Figs. 2 and 3 in Ref. [11], the appearance of the saddle at larger elongation for ^{186}Pt as compared to ^{240}Pu could give a qualitative explanation of observed asymmetry in ^{180}Hg [11]. Ichikawa *et al.* calculated the potential-energy surface for ^{180}Hg which showed only one symmetric valley at large elongation [18]. At this large elongated saddle configuration, the neck between the two preformed fragments is thin and, therefore, the fissioning system cannot access the symmetric valley. The observation of asymmetric mass distribution in the fission of ^{180}Hg prompted a series of theoretical and experimental investigations. Moller *et al.* calculated the fission fragment mass distribution for different mercury isotopes (in the mass range of 174–188) and showed that the asymmetric nature is not only restricted to ^{180}Hg, but also it could be expected for other mercury isotopes up to the excitation energy as high as 40 MeV [19]. These calculations were based on the single-particle effects in the fissioning nucleus. Calculations based on fragment shell effects by Andreev *et al.* showed that the asymmetric mass distribution in Hg isotopes could be expected even at higher excitation energies [20]. Recently, Andreev *et al.* calculated the fission fragment mass distribution in different Po and Ir isotopes at low excitation energies based on an improved scission point model [21,22]. These calculations showed both symmetric and asymmetric fission contributions in the β-delayed fission of ^{194,196}At with the major contribution being symmetric fission. For Ir isotopes, mass distributions were calculated at an excitation energy of 10 MeV above the saddle point which showed a transition from symmetric to asymmetric mass distribution whereas moving from a heavier ($A = 193$) to a lighter ($A = 185$) isotope [22]. Recently, Scamps and Simenel calculated the fragment single-particle energy states in the sublead region predicting asymmetric mass distribution [23]. These calculations were further extended to the other nuclei in Ref. [24]. The authors showed that asymmetric splitting is energetically more favorable than symmetric splitting of ^{180}Hg. Based on the calculations in Ref. [23], the observed asymmetry in the mass distribution is due to the appearance of shell gaps in the neutron and proton energy levels for fission fragments with octupole deformation at scission. These calculations predict proton shell closure in the light fragment to be the dominant driving force for the asymmetry along with the neutron shell closure in the heavy fragment.

Various experiments carried out in the mass range of $A \approx 180$ using heavy-ion induced fission showed, in general, a flat-top mass distribution which was attributed to the admixture of symmetric and asymmetric fission components [25–28]. In a recent study on the fission fragment mass distribution and total kinetic energy (TKE) in the $^{36}\mathrm{Ar} + {}^{142}\mathrm{Nd} \rightarrow {}^{178}\mathrm{Pt}$ reaction, asymmetric and symmetric fission components were associated with the different TKE values indicating contribution from different fission modes [26]. In this paper, the observed flattop mass distributions were deconvoluted into symmetric and asymmetric components by gating with different TKE values arising from the symmetric and asymmetric fission modes with an asymmetric component to be the dominant contribution in the excitation energy range of 38.6–58.4 MeV. In a study by Prasad *et al.*, a clear dip in the symmetric region in the mass distribution for ^{182}Hg was observed at an excitation energy of 33.6 MeV [28]. In light of the new theoretical developments as well as all recent experimental results, it is important to carry out extensive measurements for fissioning systems with varying neutron-proton numbers in the mass region around $A \approx 180$ at different excitation energies to understand the origin of the asymmetry in the mass distribution. It is particularly important to extend these studies to the lighter mass region for which mass distribution measurements are even more limited.

In the present paper, experiments have been carried out to determine the fission fragment mass distribution in the $^{32}\mathrm{S} + {}^{144}\mathrm{Sm}$ reaction at $E_{\mathrm{lab}} = 143.9$, 149.4, and 154.7 MeV. The present reaction system leads to the formation of the compound nucleus ^{176}Pt extending the mass distribution measurements to the lighter mass region. The excitation energy of the compound nucleus in the present paper is in the range of 38.7–47.5 MeV.

II. EXPERIMENTAL DETAILS

Experiments were carried out at the BARC-TIFR Pelletron-LINAC facility at the Tata Institute of Fundamental Research, Mumbai, India. An electrodeposited target of ^{144}Sm (enrichment $\approx 94\%$) having thickness $\approx 120\,\mu\mathrm{g/cm^2}$ on aluminum backing (thickness: $550\,\mu\mathrm{g/cm^2}$) was bombarded with a ^{32}S beam of energy 150.4, 155.9, and 161 MeV with the aluminum backing facing the beam. The beam energies obtained after accounting for the energy loss in the Al backing were 143.9, 149.4, and 154.7 MeV, corresponding to the excitation energy of the compound nucleus as 38.7, 43.2, and 47.5 MeV, respectively. Two multiwire proportional counters (MWPCs) were placed in a scattering chamber of diameter 1.5 m at the folding angle ($\theta_{\mathrm{lab}} = \pm 66.5^\circ$) for the coincident detection of the fission fragments recoiling out of the target [29]. A schematic of the experimental setup is shown in Fig. 1. From each detector, one timing and four position signals (two for X positions and two for Y positions) were fed into a time to digital converter (TDC) after introducing appropriate delays. The signals in the TDC were recorded by taking the radio-frequency (RF) signal associated with the beam pulse from the accelerator as a reference or start signal. The trigger or start signal was generated by making an "AND" gate of the RF signal with the output of the "OR" gate of timing signals from MWPCs. Two monitor detectors were placed at $\pm\ 20^\circ$ in order to detect the elastically scattered beam particles. The experimental data were acquired event by event using a VERSA-Module Euro card (VME) based multiparameter data-acquisition system [30].

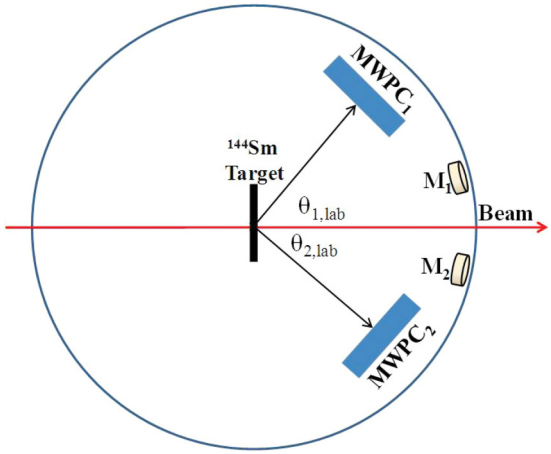

FIG. 1. Schematic of detector setup inside a general purpose scattering chamber. The two MWPCs are placed at ±66.5 °. M_1 and M_2 are the two monitors used to detect the elastically scattered beam particles.

III. DATA ANALYSIS

A plot of timing spectrum (T_1 vs T_2 where subscripts 1 and 2 represent the fragments detected in MWPC1; $\phi = 90^\circ$ and MWPC2; $\phi = 270^\circ$) for the $^{32}S + ^{144}Sm$ reaction at $E_{lab} = 149.4$ MeV is shown in Fig. 2(a). The timing spectrum was gated with fold spectra ($\theta_{1,lab}$ vs $\theta_{2,lab}$). As seen from the figure, fission events were clearly distinguished from the elastically scattered beam particles. From the knowledge of position calibration of each detector along the X and Y directions, a position (X,Y) on the detector's active area for each event was transformed into the angles (θ, ϕ) with respect to the beam direction using standard kinematics. A plot of ($\phi_2 - \phi_1$) vs ($\theta_{1,lab} + \theta_{2,lab}$) at $E_{lab} = 149.4$ MeV is shown in Fig. 2(b) where it can be seen that ($\theta_{1,lab} + \theta_{2,lab}$) is peaking at the folding angle around $\approx 133^\circ$. TOF of the fission fragments was determined using Eq. (1),

$$\mathrm{TOF} = T - T_{\mathrm{delay}} - \delta t_0, \tag{1}$$

where T is the time obtained from the time calibration of the two MWPCs. T_{delay} is the electronic delay with respect to the beam pulse (RF), which was obtained by reproducing the calculated time of flight of the elastically scattered beam particles at a particular (θ, ϕ). The TOF of the scattered beam particles was calculated using the NRV code [31]. The two MWPC detectors placed at angles ± 66.5 °, correspond to the angle of 90 ° in the center-of-mass (c.m.) frame of reference. An additional delay adjustment (δt_0) was required to make average $\theta_{c.m.} = 90^\circ$ and to make the parameter $V_\parallel/V_{CN}$ unity, where $V_\parallel$ represents the component of the c.m. velocity of the compound nucleus in the beam direction which was obtained from fragment velocities, and V_{CN} is the compound nucleus velocity as calculated from the recoil energy. $V_\parallel$ was calculated using the prescription given in Ref. [32].

The TOF values obtained using Eq. (1) were used to calculate the velocities of the fission fragments in the laboratory frame of reference. The velocities of the fission fragments were corrected for the energy loss in the target. In the present

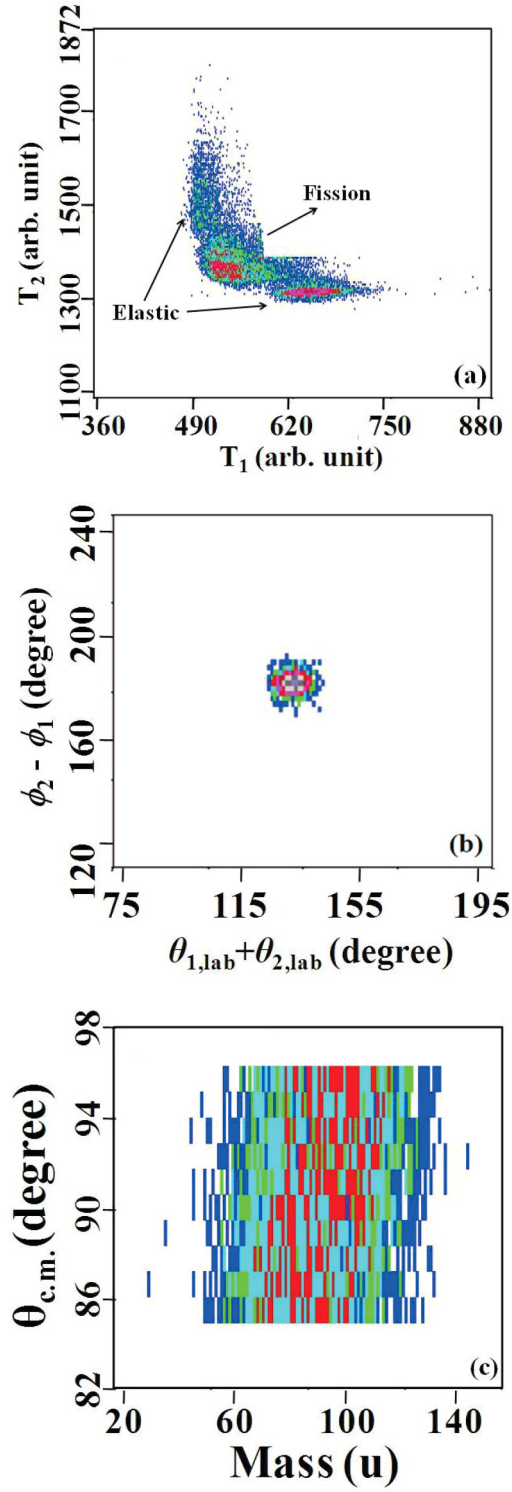

FIG. 2. (a) Plot of timing spectra for the $^{32}S + ^{144}Sm$ reaction at $E_{lab} = 149.4$ MeV. Subscripts 1 and 2 refer to two MWPCs used to detect the fission fragments. (b) Plot of ($\phi_2 - \phi_1$) vs ($\theta_{1,lab} + \theta_{2,lab}$) for the $^{32}S + ^{144}Sm$ reaction. Subscripts 1 and 2 refer to the fission fragments detected in detectors 1 and 2, respectively. (c) Plot of $\theta_{c.m.}$ vs fission fragment mass obtained in the $^{32}S + ^{144}Sm$ reaction. Due to limited angular coverage events were selected within an angular range of 85 °–95 °.

experiment, energy loss of the fission fragments was calculated using the formula $(dE/dX)_{ff} = (dE/dX)_{\text{proton}}\gamma^2 Z^2$ [33], where $(dE/dX)_{ff}$ and $(dE/dX)_{\text{proton}}$ are stopping powers of the fission fragment and proton, respectively, at the same E/A value. γ and Z are the effective charge and atomic number of the fission fragment, respectively. The effective charge of the fission fragment was obtained using the equation $\gamma = 1 - 1.032\exp(-v/v_0 Z^{0.69})$, where v refers to the velocity of the fragments as obtained from TOF measurements, and $v_0 = 2.188 \times 10^8$ cm/s is a constant term referred to as reduced velocity. The detailed procedure for the effective charge calculation can be found in Ref. [34]. The experimentally measured velocities were corrected in an iterative way until the correction did not further change the velocities significantly. The average energy loss of the fission fragment in the present system was estimated to be ≈ 3.5 MeV. The corrected velocities in the laboratory frame of reference were then transformed into the c.m. frame of reference using the standard kinematic equations. After obtaining the fission fragment velocities $V_{\text{c.m.},1}$ and $V_{\text{c.m.},2}$ in the c.m. frame of reference, fission fragment mass was calculated using the "velocity ratio method" using Eq. (2),

$$M_2 = \frac{V_{\text{c.m.1}}}{V_{\text{c.m.1}} + V_{\text{c.m.2}}} M_{\text{CN}}, \tag{2}$$

where subscripts 1 and 2 refer to the fission fragments detected in detector 1 and detector 2, respectively. M_{CN} is the mass of the compound nucleus, and M_2 is the mass of the fission fragment registered in detector 2. The mass distribution obtained by Eq. (2) was further gated with $\theta_{\text{c.m.}}$ by selecting the events in the $\theta_{\text{c.m.}}$ range of 85 °–95 ° to avoid the detector edge effect. This gate further eliminated the elastic contribution. A plot of $\theta_{\text{c.m.}}$ vs M_2 for $E_{\text{lab}} = 149.4$ MeV is shown in Fig. 2(c), which can be projected onto the X axis to obtain the mass distribution. The average TKE values obtained using the velocities of fission fragments in the c.m. frame of reference were in agreement within $\approx 10\%$ of the values obtained using the systematics in Ref. [35]. It should be mentioned here that the TKE spectra had a tailing on the higher-energy side that could not be eliminated. However, its effect on the mass distribution is expected to be insignificant as TKE has a square dependence on velocity whereas, determination of mass involves the ratio of velocities.

IV. RESULTS AND DISCUSSIONS

Plots of the fission fragment mass distributions at $E_{\text{lab}} =$ 143.9, 149.4, and 154.7 MeV are shown in Fig. 3. An upper estimate of the mass resolution was obtained from the elastic peak as ≈ 7 mass units. It can be seen from the figure that the experimental fission fragment mass distributions have a flattop nature and could not be fitted well by a one-Gaussian function. In the one-Gaussian fitting, the free parameters were area (A), centroid (c), and width (w) of the Gaussian distribution. The flattop nature of the mass distribution is consistent with the observations for similar fissioning systems indicating the contribution from multimodal fission [25,26]. As a next step, an attempt was made to fit the mass distributions as a sum of three Gaussian functions, one for symmetric fission and two

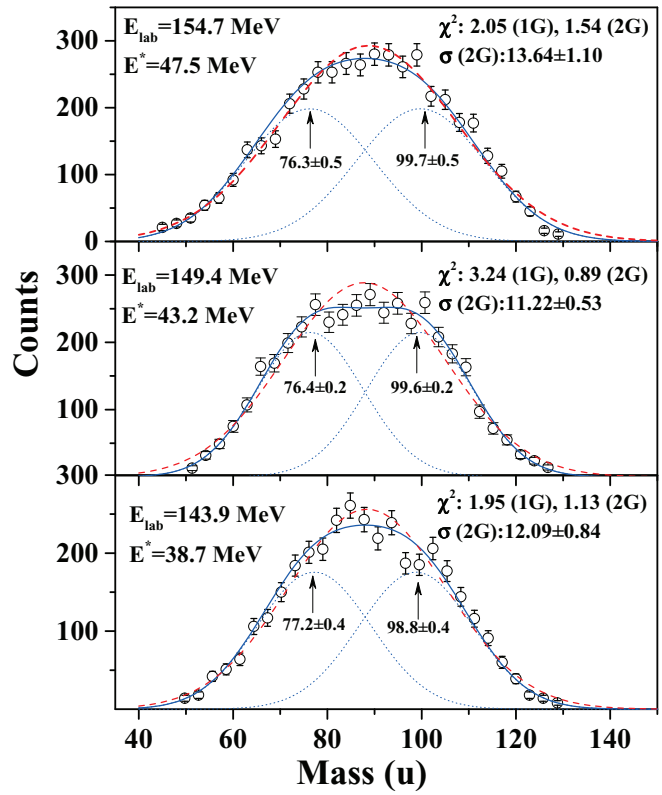

FIG. 3. Fission fragment mass distribution in the $^{32}\text{S} + ^{144}\text{Sm}$ reaction at $E_{\text{lab}} = 143.9$, 149.4, and 154.7 MeV. The open circles are the experimental data points. The red dashed lines represent the one-Gaussian (1G) fitting, and blue lines represent the two-Gaussian (2G) fitting. The χ^2 values for one-Gaussain and two-Gaussian fittings are given in the figure. The corresponding excitation energies of the compound nucleus are mentioned in the figure. The centroid values for two-Gaussian fitting are also marked in the figure.

for asymmetric fission. However, such a three-Gaussian fitting resulted in a symmetric component with a very large uncertainty on its magnitude and prohibited a realistic estimate of the symmetric fission component. Therefore, as an approximation, the mass distribution was fitted to a two-Gaussian function to extract the centroid values corresponding to the asymmetric fission components. In the two-Gaussian fitting, the total number of parameters was reduced to three by imposing the conditions that: (i) centroid of the second peak $c_2 = 176c_1$ (c_1: centroid of the first peak), and (ii) w and area of the two asymmetric peaks are equal which implies that $w_1 = w_2$ and $\text{area}_1 = \text{area}_2$. The χ^2 values obtained in the one-Gaussian and two-Gaussian fittings are given in Fig. 3. It can be seen from the figure that there is a significant improvement in the χ^2 values in the two-Gaussian fitting as compared to the one-Gaussian fitting at all three beam energies corresponding to the excitation energy range of 38.7–47.5 MeV. The centroid values for heavy and light mass peaks obtained in the two-Gaussian fitting are also marked in Fig. 3. The values obtained in the present paper were observed to be close to those obtained in similar compound nucleus system ^{178}Pt [26]. A series of recent measurements has experimentally confirmed the flattop nature of the mass distribution which

has been attributed to the contribution from symmetric and asymmetric fission components [16,17,25–28].[1]

Extensive theoretical studies have been carried out to understand the origin of this asymmetry in the mass distribution by relating it to single-particle effects in the fissioning nucleus or fission fragments [19,20]. Based on the five-dimensional (5D) potential-energy calculations as described in Refs. [7,37], the most probable split in the asymmetric fission of ^{180}Hg is expected to be 108/72. Randrup and Moller modified the 5D calculation model with random-walk approximation in order to consider the dynamical aspects for the evolution of the fissioning system from the ground state to the separated fragments [38]. Based on this modified approach Moller *et al.* calculated the fission fragment mass distributions for different Hg isotopes and predicted the most probable mass split in the fission of ^{180}Hg to be 104.4/75.6 [19]. Recent calculations by Ichikawa and Moller [11] relate the asymmetry in the mass distribution of ^{180}Hg to the interaction of the [30$\Lambda\Omega$] and [41$\Lambda\Omega$] levels of the fissioning nucleus, similar to that predicted in Ref. [10] for nuclei in the rare-earth region. In the βDF, the observed mass split was 100/80 [16,17]. Calculations by Andreev *et al.* showed asymmetric mass distribution for ^{185}Ir with a heavy fragment peak around the mass number $\approx$ 100 [22]. Scamps and Simenel calculated the single-particle energy states for the fragments at scission with quadrupole and octupole deformations in the sublead region [23]. These calculations showed that the asymmetric splitting is energetically more favorable than symmetric division for ^{180}Hg. In these calculations for the fissioning systems in the mass range of $A \approx 176$–184, it was shown that $Z_L \approx 34$–36 and $N_H \approx 56$ is responsible for the observed asymmetry. Subsequently, based on further calculations for more fissioning systems, it was proposed that proton shell closure in the light fragment at scission plays the dominant role [24]. In this paper, the appearance of a shell gap at $Z_L \approx 34$ for $N_L < 50$ (N_L: neutron number of the lighter fragment) and $Z_L \approx 38$ for $N_L > 50$ has been proposed.

In order to investigate the dependence of the centroid values of light and heavy mass peaks of the mass distribution on the fissioning system, a comparison of the data from the present paper along with those from ^{35}Cl + ^{144}Sm → ^{179}Au [25], ^{36}Ar + ^{142}Nd → ^{178}Pt [26], ^{36}Ar + ^{144}Sm → ^{180}Hg [27], and ^{40}Ca + ^{142}Nd → ^{182}Hg [28] reaction systems and βDF of ^{180}Tl [16] has been carried out. For comparison, data corresponding to the lowest excitation energy were taken from these heavy-ion induced reactions, which span over an excitation energy range of 33.6–38.7 MeV for different systems. The data from ^{35}Cl + ^{144}Sm was subjected to a two-Guassian fitting to obtain the centroid values of the asymmetric peaks. Figure 4 shows a plot of the centroid values of the heavy (A_H) and light (A_L) mass peaks as a function of the compound nucleus mass. It is interesting to note from the figure that the value of A_H remains nearly constant, whereas A_L slowly increases with an increase in the mass of the compound nucleus, an observation similar to that from the low-energy fission of actinides. In view of recent theoretical calculations, this was further investigated by determining the corresponding neutron and proton numbers. Assuming that the fragments have the same neutron to proton ratio as that of the compound nucleus, the corresponding $Z_H(Z_L)$ values were obtained as $A_H(A_L)Z_{CN}/A_{CN}$, where Z_{CN} and A_{CN} are the compound nucleus charge and mass, respectively. Subsequently, the neutron numbers $N_H(N_L)$ were obtained as $A_H(A_L) - Z_H(Z_L)$. A plot of neutron and proton numbers corresponding to A_H and A_L is shown in Fig. 5. The dashed lines correspond to the mean values, and the solid line is a linear fit to the data. It should be mentioned here that the neutron and the proton numbers are correlated as they have been obtained by imposing the condition of the same *A/Z* value for the fragment and fissioning system. Furthermore, N_H (or Z_H) and N_L (or Z_L) values are expected to follow the trends similar to that of A_H and A_L, respectively, as *A/Z* ratios of the compound nuclei included in the analysis are not very different. It can be seen from Fig. 5 that the N_H value is close to $\approx$ 56 and Z_L is in the range of $\approx$ 34–36 in the compound nucleus mass region 176–182. This is in agreement with the prediction for this mass range in Refs. [23,24], which is based on the fragment shell effects at scission.

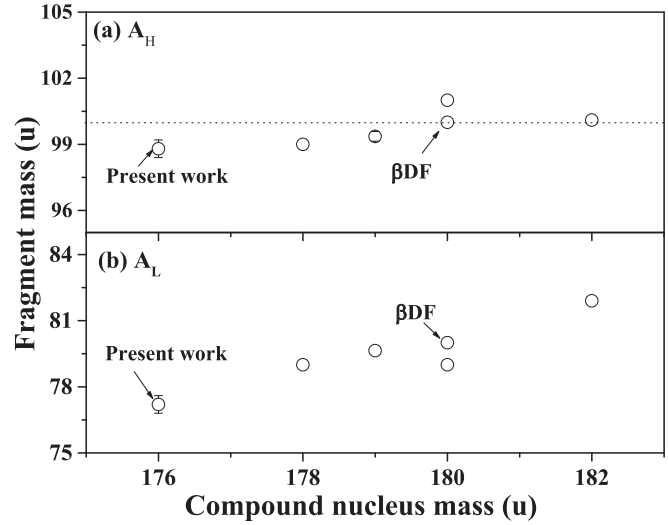

FIG. 4. Plot of centroid values of the (a) heavy (A_H) and the (b) light (A_L) mass peaks of fission fragment mass distribution for different reaction systems [16,25–28] populating compound nuclei around the mass region $A \approx 180$, including the data from the present paper as a function of the compound nucleus mass. The dotted line represents the average fragment mass $A \approx 100$. Data from the present paper are marked by arrows.

Fission fragment mass distributions in the present experiment have been calculated based on the prescission configuration using the code GEF (version: GEF 2020/1.1) [39]. In GEF calculations, excitation energy and the average angular momentum were supplied as input parameters. A comparison

[1]Towards the end of the review process, it came to our attention that a parallel independent measurement for the present system (^{32}S + ^{144}Sm → ^{176}Pt) has also been carried out by another group and has been published in Ref. [36]. Importantly, the conclusions from the two studies are mutually consistent.

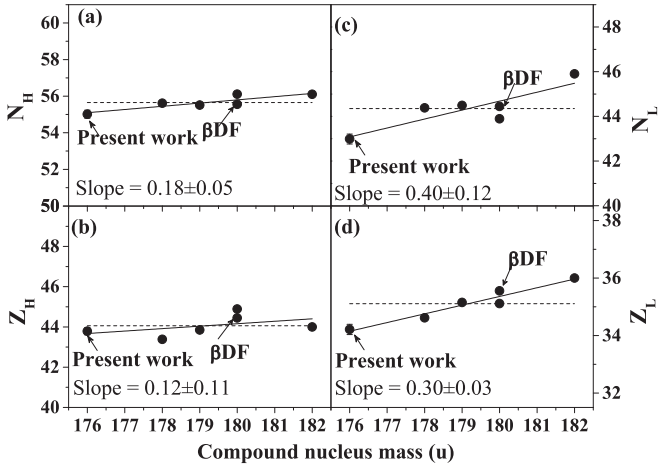

FIG. 5. Plot of neutron and proton numbers corresponding to the centroid values of light and heavy mass peaks for asymmetric fission for different fissioning systems [16,25–28] along with the data from the present paper which are marked by arrows. $N_L(Z_L)$ and $N_H(Z_H)$ represent the neutron (proton) numbers corresponding to centroid values for light and heavy mass peaks, respectively.

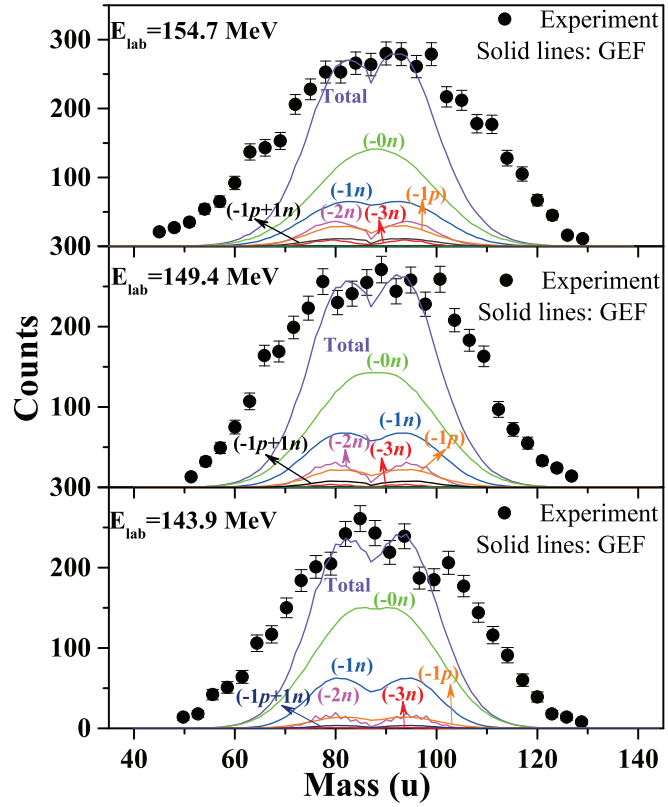

FIG. 6. Fission fragment mass distribution in the $^{32}S + ^{144}Sm$ reaction. Filled circles are the experimental data points, and solid lines are the GEF calculations. The mass distributions corresponding to the different chance fissions are marked in the figure.

of experimental mass distributions at $E_{lab} = 143.9$, 149.4, and 154.7 MeV with those calculated using GEF has been shown in Fig. 6. The data from GEF calculations have been normalized in the peak region with the experimental data. In the present paper the excitation energy of the compound nucleus (^{176}Pt) is in the range of 38.7–47.5 MeV as given in Table I. In this excitation energy range, the compound nucleus may undergo multichance fission. In order to investigate the effect of proton and neutron evaporations, mass distributions have been calculated for different chance fissions using the code GEF, which is shown in Fig. 6. The peak to valley (P/V) ratio in the calculated mass distributions is gradually increasing with increasing the number of emitted neutrons and protons as shown in Fig. 6, which can be related to the decreasing excitation energy. It can be seen from this figure that the fission followed by neutron emission constitutes the major contribution compared to the fission followed by charged particle evaporation. Based on GEF calculations, a major fission contribution arises from first chance fission which is 68%, 60%, and 56% at $E_{lab} = 143.9$, 149.4, and 154.7 MeV, respectively. The contribution from second chance fission is about $\approx 23\%$ at all beam energies. The rest is contributed by higher chance fission. In the present paper, the average angular momentum ($\langle l \rangle$) values, calculated using the code CCFUS [40], were 15, 22, and 27$\hbar$ at $E_{lab} = 143.9$, 149.4, and 154.7 MeV, respectively. Fission barriers corresponding to average angular momentum as well as for $l = 0$, calculated using the rotating liquid drop model [41], are given in Table I. It can be seen from the table that the fission barrier (B_f) obtained for $l = 0$ has reasonably good agreement with the B_f value from Ref. [42] based on the 5D potential-energy calculation. Furthermore, with increasing angular momentum, there is a gradual decrease in the fission barrier from 11.50 to 9.69 MeV,

TABLE I. Values of different reaction parameters for the $^{32}S + ^{144}Sm$ reactions at $E_{lab} = 143.9$, 149.4, and 154.7 MeV. The values of E_{lab} have been obtained after correcting for the beam energy loss in the target backing and have been used to obtain the excitation energy of the compound nucleus (E^*_{CN}). The average angular momenta of the compound nucleus ($\langle l \rangle$) at different beam energies have been calculated using the code CCFUS [40]. Fission barrier (B_f) values corresponding to the average angular momenta have been calculated using the rotating liquid drop model [41]. The corresponding fissility (χ) values have been calculated using the procedure given in Ref. [43]. The fission barrier values for $l = 0$ as obtained using the rotating liquid drop model [41] and from more recent five-dimensional potential-energy calculation as given in Ref. [42] are given in the last two columns, respectively.

E_{lab} (MeV)	E^*_{CN} (MeV)	$\langle l \rangle (\hbar)$	B_f (MeV) [41]	Fissility (χ) [43]	B_f ($l = 0$) (MeV) [41]	B_f ($l = 0$) (MeV) [42]
143.9	38.7	15	11.50	0.718	12.37	12.38
149.4	43.2	22	10.55	0.725		
154.7	47.5	27	9.69	0.732		

which is not very significant. The reduction in the fission barrier can be considered as an increase in the fissility (χ) of the compound nucleus with increasing beam energy [43]. The fissility would change from 0.718 to 0.732 corresponding to a change in the average angular momentum from 15 to 27$\hbar$, which is a small change. Thus, the variation in the average angular momentum values over a small beam energy range of the present paper is not likely to cause any significant change in the mass distribution with variation in beam energy. The variation in the contribution from first chance fission from 68% to 56% from lowest to highest beam energies is primarily due to the increase in the excitation energy which would open up higher chance fission. However, it should be mentioned here that modification of the potential-energy surface for large l waves close to $l_{\max}$ can affect the entrance channel dynamics governing the contribution from nonequilibrium fission, although it is difficult to get a quantitative estimate of this contribution. The larger widths of the experimental mass distributions compared to the GEF calculations suggest the role of shell effects corresponding to higher mass asymmetry values as compared to those considered in GEF calculations in addition to the effects possibly arising from the entrance channel dynamics. A similar observation was made by Gupta *et al.* in the study of fission fragment mass distribution for ^{191}Au and was attributed to the entrance channel dynamics [44]. This was further supported by the observation of the larger width of the fission fragment mass distribution in the $^{37}\mathrm{Cl} + {}^{154}\mathrm{Sm}$ reaction compared to that in the $^{16}\mathrm{O} + {}^{175}\mathrm{Lu}$ reaction populating the same compound nucleus ^{191}Au [44]. For the compound nucleus ^{176}Pt, which has 12 neutrons and 3 protons less compared to the compound nucleus reported in Ref. [44], it is difficult to have conclusive information on this aspect, particularly, in the absence of the data for a complementary reaction system with higher entrance channel mass asymmetry as in the case of ^{191}Au [44]. In order to investigate the dependence of the entrance channel effect on the Z_PZ_T (Z_P and Z_T are the proton numbers of the projectile and the target, respectively) value of the reaction systems specific to mass region ≈ 180, a comparison of the width (σ) of mass distributions from different reaction systems with Z_PZ_T values in the range of 992–1200 [25–28], including the data from the present measurement, is shown in Fig. 7. As these mass distributions cannot be fitted well by a one-Gaussian function, the σ values were obtained as $[C_i(M_{R,i} - 0.5)^2/\sum C_i]^{1/2}$, where C_i represents the counts corresponding to specific mass ratio i. The excitation energy values of the compound nuclei are also given in the figure. For all the systems included in comparison, data correspond to the similar $E_{\mathrm{c.m.}}/V_C$ values except for the $^{40}\mathrm{Ca} + {}^{142}\mathrm{Nd} \rightarrow {}^{182}$Hg system [28]. Therefore, additional data for this system at higher beam energy has also been included for comparison. From Fig. 7, it can be seen that the mass distribution for the present reaction system ($^{32}\mathrm{S} + {}^{144}\mathrm{Sm}$) is relatively broader as compared to other systems, except the $^{40}\mathrm{Ca} + {}^{142}\mathrm{Nd} \rightarrow {}^{182}$Hg system at deep sub-barrier energy corresponding to excitation energy of 33.6 MeV. Observation of the large width for $^{40}\mathrm{Ca} + {}^{142}\mathrm{Nd} \rightarrow {}^{182}$Hg at lower beam energy compared to that at higher beam energy suggests the pronounced effect of the entrance channel dynamics at deep sub-barrier energy in addition to single-particle effects. Furthermore, the larger width for the present reaction system with the lowest Z_PZ_T compared to the other systems at similar $E_{\mathrm{c.m.}}/V_C$ values shows the importance of the role played by the neutron-proton configuration of the fissioning system in addition to the entrance channel dynamics.

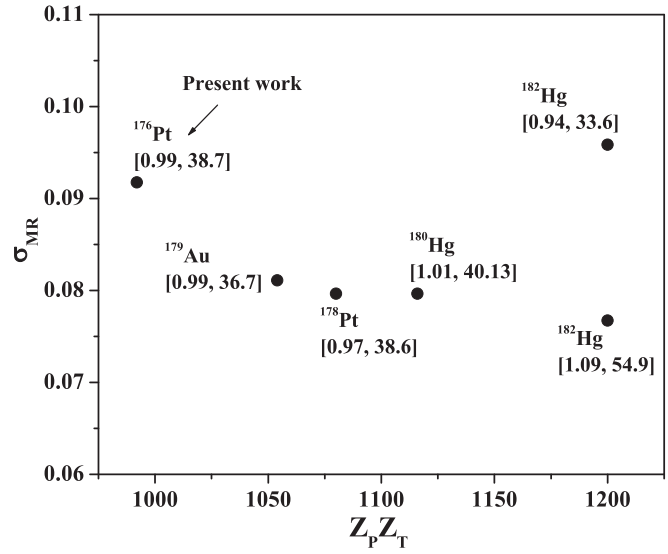

FIG. 7. Plot of σ_{MR} values obtained from the present paper along with the values obtained from literature data on mass distribution for different compound nuclei (^{179}Au [25], ^{178}Pt [26], ^{180}Hg [27], and ^{182}Hg [28]) in the mass region $A \approx 180$ as a function of Z_PZ_T. The ratio of projectile energy in the c.m. frame of reference to the entrance channel Coulomb barrier ($E_{\mathrm{c.m.}}/V_C$) and excitation energy (in MeV) of the compound nucleus for different reaction systems are mentioned in the brackets.

V. CONCLUSIONS

Fission fragment mass distributions have been obtained for the $^{32}\mathrm{S} + {}^{144}\mathrm{Sm}$ reaction system at beam energies of 143.9, 149.4, and 154.7 MeV corresponding to the $E_{\mathrm{c.m.}}/V_C \approx 0.99$, 1.04, and 1.07, respectively. The mass distributions at all the three beam energies were observed to have a flattop nature indicating the contribution from multimodal fission. The experimental mass distributions could not be fitted well with a one-Gaussian function. The two-Gaussian function gave a better fit with considerably lower χ^2 values. An analysis of the centroid values of light and heavy mass peaks as obtained from the present paper along with those extracted from the literature data in the mass region 176–182 showed that the centroid value for the heavy mass peak remains nearly constant at ≈ 100 whereas that for the light mass peak increases with increasing mass of the fissioning system. A further analysis of the corresponding neutron-proton numbers revealed that the heavy fragment neutron number is nearly constant around $N_{\mathrm{H}} \approx 56$ and the light fragment proton number is in the range of $Z_{\mathrm{L}} \approx 34$–36. This is consistent with the predictions in Refs. [23,24] for the mass region 176–182 based on fragment shell effects at scission. A comparison of the width of the mass distributions from fissioning systems with different

$Z_P Z_T$ values shows that, in addition to the entrance channel dynamics, the neutron-proton configuration of the fissioning system plays an important role in governing the overall mass distribution.

[1] R. Vandenbosch and J. R. Huizenga, *Nuclear Fission* (Academic, New York, 1973).
[2] C. F. Tsang and J. B. Wilhelmy, Nucl. Phys. **A184**, 417 (1972).
[3] C. Wagemans, *The Nuclear Fission Process* (CRC, London, 1991).
[4] S. Sodaye, R. Tripathi, K. Sudarshan, and R. Guin, Phys. Rev. C **87**, 044610 (2013).
[5] S. Sodaye, R. Tripathi, B. V. John, K. Ramachandran, and P. K. Pujari, Phys. Rev. C **95**, 014612 (2017).
[6] T. N. Nag, R. Tripathi, S. Sodaye, K. Sudarshan, K. Ramachandran, B. K. Nayak, and P. K. Pujari, Phys. Rev. C **96**, 044608 (2017).
[7] P. Moller, D. G. Madland, A. J. Sierk, and A. Iwamoto, Nature (London) **409**, 785 (2001).
[8] V. M. Strutinsky, Nucl. Phys. **A95**, 420 (1967).
[9] N. Bohr and J. A. Wheeler, Phys. Rev. **56**, 426 (1939).
[10] C. Gustafsson, P. Moller, and S. G. Nilsson, Phys. Lett. B **34**, 349 (1971).
[11] T. Ichikawa and P. Moller, Phys. Lett. B **789**, 679 (2019).
[12] P. Moller and S.G. Nilsson, Phys. Lett. B **31**, 283 (1970).
[13] H. C. Pauli, T. Ledergerber, and M. Brack, Phys. Lett. B **34**, 264 (1971).
[14] M. G. Itkis, N. A. Kondrat'ev, and S. I. Mul'gin, Yad. Fiz. **52**, 944 (1990).
[15] M. G. Itkis, N. A. Kondrat'ev, S. I. Mul'gin, V. N. Okolovich, A. Ya. Rusanov, and G. N. Smirenkin, Yad. Fiz. **53**, 1225 (1991).
[16] A. N. Andreyev, J. Elseviers, M. Huyse, P. Van Duppen, S. Antalic, A. Barzakh, N. Bree, T. E. Cocolios, V. F. Comas, J. Diriken, D. Fedorov, V. Fedosseev, S. Franchoo, J. A. Heredia, O. Ivanov, U. Koster, B. A. Marsh, K. Nishio, R. D. Page, N. Patronis, M. Seliverstov, I. Tsekhanovich, P. Van den Bergh, J. Van De Walle, M. Venhart, S. Vermote, M. Veselsky, C. Wagemans, T. Ichikawa, A. Iwamoto, P. Moller, and A. J. Sierk, Phys. Rev. Lett. **105**, 252502 (2010).
[17] J. Elseviers, A. N. Andreyev, M. Huyse, P. Van Duppen, S. Antalic, A. Barzakh, N. Bree, T. E. Cocolios, V. F. Comas, J. Diriken, D. Fedorov, V. N. Fedosseev, S. Franchoo, L. Ghys, J. A. Heredia, O. Ivanov, U. Koster, B. A. Marsh, K. Nishio, R. D. Page, N. Patronis, M. D. Seliverstov, I. Tsekhanovich, P. Van den Bergh, J. Van De Walle, M. Venhart, S. Vermote, M. Veselsky, and C. Wagemans, Phys. Rev. C **88**, 044321 (2013).
[18] T. Ichikawa, A. Iwamoto, P. Moller, and A. J. Sierk, Phys. Rev. C **86**, 024610 (2012).
[19] P. Moller, J. Randrup, and A. J. Sierk, Phys. Rev. C **85**, 024306 (2012).
[20] A. V. Andreev, G. G. Adamian, and N. V. Antonenko, Phys. Rev. C **86**, 044315 (2012).
[21] A. V. Andreev, G. G. Adamian, N. V. Antonenko, S. P. Ivanova, and W. Scheid, Eur. Phys. J. A **22**, 51 (2004).
[22] A. V. Andreev, G. G. Adamian, and N. V. Antonenko, Phys. Rev. C **93**, 034620 (2016).
[23] G. Scamps and C. Simenel, Phys. Rev. C **100**, 041602(R) (2019).
[24] K. Mahata, C. Schmitt, S. Gupta, A. Shrivastava, G. Scamps, and K.-H. Schmidt, arXiv:2007.16184.
[25] R. Tripathi, S. Sodaye, K. Sudarshan, B. K. Nayak, A. Jhingan, P. K.Pujari, K. Mahata, S. Santra, A. Saxena, E. T. Mirgule, and R. G. Thomas, Phys. Rev. C **92**, 024610 (2015).
[26] I. Tsekhanovich, A. N. Andreyev, K. Nishio, D. Denis-Petit, K. Hirose, H. Makii, Z. Matheson, K. Morimoto, K. Morita, W. Nazarewicz, R. Orlandi, J. Sadhukhan, T. Tanaka, M. Vermeulen, and M. Warda, Phys. Lett. B **790**, 583 (2019).
[27] K. Nishio, A. N. Andreyev, R. Chapman, X. Derkx, C. E. Dullmann, L. Ghys, F. P. Hessberger, K. Hirose, H. Ikezoe, J. Khuyagbaatar, B. Kindler, B. Lommel, H. Makii, I. Nishinaka, T. Ohtsuki, S. D. Pain, R. Sagaidak, I. Tsekhanovich, M. Venhart, Y. Wakabayashi, and S. Yan, Phys. Lett. B **748**, 89 (2015).
[28] E. Prasad, D. J. Hinde, K. Ramachandran, E. Williams, M. Dasgupta, I. P. Carter, K. J. Cook, D. Y. Jeung, D. H. Luong, S. McNeil, C. S. Palshetkar, D. C. Rafferty, C. Simenel, A. Wakhle, J. Khuyagbaatar, Ch. E. Dullmann, B. Lommel, and B. Kindler, Phys. Rev. C **91**, 064605 (2015).
[29] A. Pal, S. Santra, A. Kundu, D. Chattopadhyay, A. Jhingan, B. K. Nayak, and S. Prafulla, J. Instrum. **15**, P02008 (2020).
[30] A. Kumar, A. Chatterjee, K. Mahata, and K. Ramachandran, *Development of Data Acquisition Software for VME Based System, 9th International Workshop on Personal, Computers and Particle Accelerators, Kolkata, India, 2012* (Curran, Red Hook, NY, 2012), pp. 35–36.
[31] www.nrv.jinr.ru.
[32] D. J. Hinde, M. Dasgupta, J. R. Leigh, J. C. Mein, C. R. Morton, J. O. Newton, and H. Timmers, Phys. Rev. C **53**, 1290 (1996).
[33] L. C. Northcliffe and R. F. Schilling, Nucl. Data Tables, Sect. A **7**, 233 (1970).
[34] H.-D. Betz, Rev. Mod. Phys. **44**, 465 (1972).
[35] V. E. Viola, K. Kwiatkowski, and M. Walker, Phys. Rev. C **31**, 1550 (1985).
[36] E. Prasad, D. J. Hinde, M. Dasgupta, D. Y. Jeung, A. C. Berriman, B. M. A. Swinton-Bland, C. Simenel, E. C. Simpson, R. Bernard, E. Williams, K. J. Cook, D. C. Rafferty, C. Sengupta, J. F. Smith, K. Vo-Phuoc, and J. Walshe, Phys. Lett. B **811**, 135941 (2020).
[37] P. Moller, A. J. Sierk, T. Ichikawa, A. Iwamoto, R. Bengtsson, H. Uhrenholt, and S. Aberg, Phys. Rev. C **79**, 064304 (2009).
[38] J. Randrup and P. Moller, Phys. Rev. Lett. **106**, 132503 (2011).
[39] K. H. Schmidt, B. Jurado, C. Amouroux, and C. Schmitt, Nuclear Data Sheets **131**, 107 (2016).
[40] C. H. Dasso and S. Landowne, Comput. Phys. Commun. **46**, 187 (1987).
[41] A. J. Sierk, Phys. Rev. C **33**, 2039 (1986).
[42] P. Moller, A. J. Sierk, T. Ichikawa, A. Iwamoto, and M. Mumpower, Phys. Rev. C **91**, 024310 (2015).
[43] R. Tripathi, K. Sudarshan, A. Goswami, P. K. Pujari, B. S. Tomar, and S. B. Manohar, Phys. Rev. C **69**, 024613 (2004).
[44] S. Gupta, K. Mahata, A. Shrivastava, K. Ramachandran, S. K. Pandit, P. C. Rout, V. V. Parkar, R. Tripathi, A. Kumar, B. K. Nayak, E. T. Mirgule, A. Saxena, S. Kailas, A. Jhingan, A. K. Nasirov, G. A. Yuldasheva, P. N. Nadtochy, and C. Schmitt, Phys. Lett. B **803**, 135297 (2020).